Electrochemistry of Individual Monolayer Graphene Sheets

Wan Li,[†] Cen Tan,[‡] Michael A. Lowe,[‡] Héctor D. Abruña,[‡,*] and Daniel C. Ralph[†,*]

[†]Department of Physics and Kavli Institute at Cornell and [‡]Department of Chemistry and Chemical Biology, Cornell University, Ithaca, New York 14853, United States

ABSTRACT We report on the fabrication and measurement of devices designed to study the electrochemical behavior of individual monolayer graphene sheets as electrodes. We have examined both mechanically exfoliated and chemical vapor deposited (CVD) graphene. The effective device areas, determined from cyclic voltammetric measurements, show good agreement with the geometric area of the graphene sheets, indicating that the redox reactions occur on clean graphene surfaces. The electron transfer rates of ferrocenemethanol at both types of graphene electrodes were found to be more than 10-fold faster than at the basal plane of bulk graphite, which we ascribe to corrugations in the graphene sheets. We further describe an electrochemical investigation of adsorptive phenomena on graphene surfaces. Our results show that electrochemistry can provide a powerful means of investigating the interactions between molecules and the surfaces of graphene sheets as electrodes.

KEYWORDS: electrochemistry · graphene · charge transfer · desorption · cyclic voltammetry

Graphene has received widespread attention due to its unique electronic, mechanical, and optical properties.[1,2] As a single layer of carbon atoms, graphene is two-dimensional and fully composed of surfaces. Thus, surface chemistry plays a major role in determining its properties. For example, molecules and atoms adsorbed on graphene surfaces are known to serve as local doping sites that significantly alter graphene's electronic properties.[3,4] Several techniques have been developed to study the interactions between molecules and graphene surfaces. For example, Raman spectroscopy has been widely employed to characterize the quality of the graphene surface and to detect molecules bound to graphene,[5−7] and scanning tunneling microscopy has been used to image molecules on graphene.[8] However, these techniques provide limited information about the *kinetics* of graphene−molecule interactions.

Electrochemistry provides a means to measure electron transfer kinetics and interactions between molecules and electrode surfaces.[9−11] Carbon materials, in various forms, have been extensively used as electrodes in both academic studies and industrial applications.[12] In particular, electrochemical studies on novel forms of carbon materials, including carbon nanotubes,[13,14] fullerene films,[15] and doped diamond,[16] have revealed rich surface chemistry. Recent electrochemical studies on chemically synthesized graphene pastes suggest that graphene may have favorable electron transfer kinetics.[17−21] However, these studies were restricted to powders of synthesized graphene flakes attached to Pt or glassy carbon electrodes, and questions remain as to whether the improved electron transfer kinetics simply reflects an increase in the microscopic surface areas.[22] The electrochemistry of and at individual monolayer graphene sheets has not been reported previously.

Here we report on the fabrication and study of devices in which a well-defined area of single-layer graphene served as the working electrode in electrochemical experiments. We examined both mechanically exfoliated graphene and chemical vapor deposited (CVD) graphene, with a focus on investigating the interactions between graphene and the simple redox molecule ferrocenemethanol (FcMeOH). Mechanically exfoliated graphene was chosen for its advantage of being a single crystal with the least density of defects, while CVD graphene[23,24] provides large areas, good uniformity, and is relatively easily transferred to a SiO_2 substrate and so provides a promising way for volume production of devices. We used cyclic voltammetric measurements to characterize the effective areas of the graphene devices and found good agreement with the geometric area of the graphene sheets, indicating that the redox reactions occur on clean, well-defined areas of graphene surface. We were thus able to use electrochemical techniques to characterize the electron transfer rates between FcMeOH and graphene, finding

* Address correspondence to hda1@cornell.edu, ralph@ccmr.cornell.edu.

Received for review December 20, 2010 and accepted February 10, 2011.

Published online February 18, 2011
10.1021/nn103537q

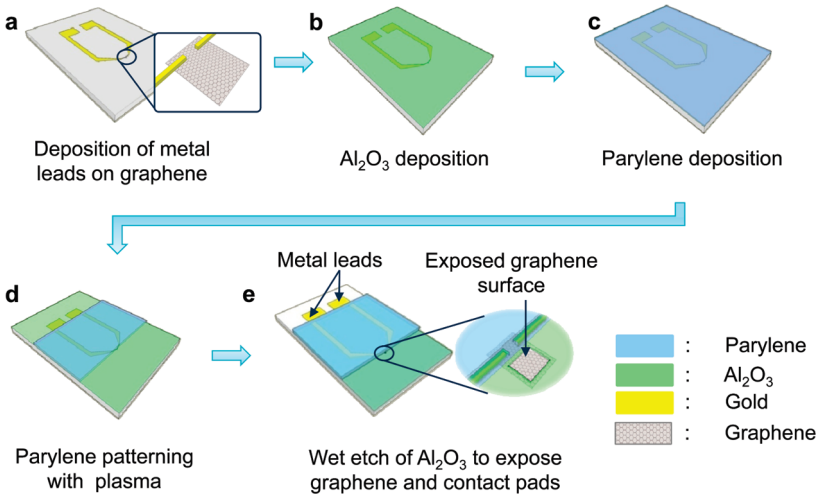

Figure 1. Procedure for fabricating monolayer graphene sheets into working electrodes for electrochemical characterization.

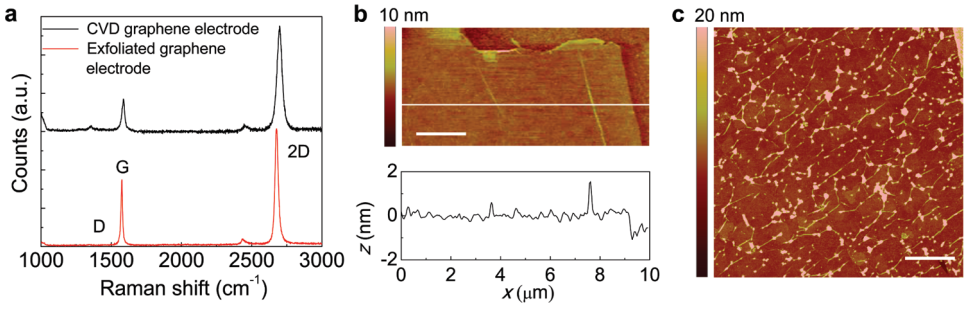

Figure 2. Raman and AFM characterization of the graphene working electrodes. (a) Raman spectra of the graphene working electrodes, after the device fabrication process was completed. (b) AFM image of the surface of a working electrode made of exfoliated graphene. A cross-sectional profile is given for the line in the top panel. Scale bar: 2 μm. (c) AFM image of the surface of a working electrode made of CVD graphene. Note that the entire area in (c) is within the surface of the CVD graphene electrode. Scale bar: 2 μm.

interesting differences relative to analogous measurements on bulk graphite. In addition, we further demonstrate the real-time electrochemical detection of molecular desorption from graphene surfaces.

RESULTS AND DISCUSSION

Figure 1 illustrates the structure of our devices and the fabrication scheme. A monolayer graphene sheet was first deposited onto a SiO_2-coated Si substrate. As noted above, two types of graphene, namely, mechanically exfoliated graphene and CVD graphene, were investigated. For both types of graphene, optical lithography was then employed to connect each piece of graphene to at least two metal leads (Figure 1a). A resistance of ~1 kΩ was typically found in two-point measurements between the leads, indicating good contacts to the graphene. A 100 nm Al_2O_3 layer (Figure 1b), followed by a 600 nm parylene layer (Figure 1c), was deposited to isolate the metal leads from the solution in electrochemical experiments. An oxygen plasma was employed to remove a region of the parylene layer above the graphene while keeping the metal leads covered (Figure 1d). Finally, a window through the Al_2O_3 layer was made using a wet etch to expose a well-defined area of the graphene surface (Figure 1e). This design ensures that graphene is the only electrochemically active surface that is in contact with the solution during electrochemical measurements. In addition, the fabrication steps were chosen to minimize the likelihood of contaminating the graphene. The maximum sizes of the exposed graphene surfaces were ~15 × 15 μm^2 for the mechanically exfoliated graphene and ~0.38 × 0.50 mm^2 for the CVD graphene since CVD graphene can be formed in much larger sheets than exfoliated graphene. In the final step, vacuum annealing at 350 °C was used in an attempt to remove organic residuals which might have remained on the graphene surface after processing. A related device design has been used previously to study the quantum capacitance of graphene.[25]

The fabricated graphene electrodes were characterized using multiple methods to confirm the quality and cleanliness of the graphene surface. Figure 2a shows micro-Raman spectra of the graphene working electrodes after the device fabrication process was completed. For both types of graphene, a symmetric single peak is observed for the 2D band, whose peak intensity is significantly higher than the G peak. These results

confirm that the graphene electrodes investigated in this study are high-quality single layers.[26] For electrodes made of mechanically exfoliated graphene, no observable D peak was evident at ~1350 cm^{-1}, indicating that the graphene sheet is clean and (at the resolution limit of micro-Raman) defect-free. In comparison, a small D peak is observed for electrodes made of CVD graphene,[27−29] indicating a less pristine layer, as is generally the case for such samples.

Atomic force microscopy (AFM) images of the devices further confirmed these observations. Dust- and dirt-free surfaces (rms roughness ~180 pm away from the larger wrinkles) were observed for electrodes made of exfoliated graphene sheets (Figure 2b). Nanoscale surface corrugations, known to be intrinsic to graphene sheets,[30,31] were clearly evident, in addition to wrinkle-like structures[32] visible in the cross-sectional profile in Figure 2b. The step height of the graphene layer with respect to the SiO_2 substrate was ~0.8 nm, in good agreement with the known value for clean graphene (0.5 to 1 nm).[33] In comparison, electrodes made of CVD graphene sheets were more disordered—features including larger wrinkles, particulates, and domain-like structures were observed following the CVD growth and transfer process (Figure 2c).[23]

We now turn to a discussion of the electrochemical measurements. Figure 3a shows cyclic voltammograms measured using an exfoliated graphene electrode in FcMeOH solution at different scan rates. FcMeOH was chosen for this study for its simple redox behavior (one-electron outer sphere process) and good chemical stability in an aerobic aqueous environment. We observed sigmoidal voltammograms and scan-rate-independent limiting steady-state currents, both characteristic of radial diffusion at ultramicroelectrodes.[11,34] This is in agreement with the graphene electrode area, which had lateral dimensions smaller than the characteristic length used to define an ultramicroelectrode (~25 μm).[11] The slight hysteresis in the forward and reverse sweeps is due to the relatively large capacitance of the graphene electrode device when compared to the current level.[11] In the following discussion, we used the cyclic voltammogram measured at the slowest scan rate, and carefully subtracted the background to eliminate the influence of the capacitance. According to the planar disk ultramicroelectrode model,[11] the effective area (A_{eff}) of an ultramicroelectrode is related to the steady-state current (i_{ss}) by

$$A_{eff} = \pi \left(\frac{i_{ss}}{4nFDC_0^*} \right)^2 \quad (1)$$

where $C_0^* = 5.2$ mM is the FcMeOH concentration, $D = 7.4 \times 10^{-6}$ cm^2/s is the diffusion constant of FcMeOH,[35] $n = 1$ is the number of electrons involved in the redox reaction, and F is the Faraday constant. From the experimental i_{ss} (9.01 nA), we calculate the

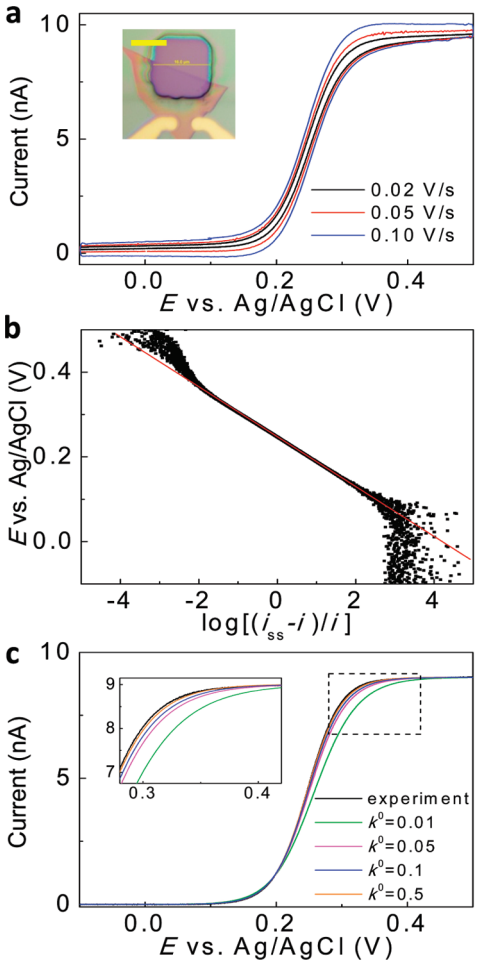

Figure 3. Electrochemistry at an exfoliated graphene electrode. (a) Voltammograms of FcMeOH (5.2 mM) in H_2O/1 M KCl at an exfoliated graphene electrode at different potential scan rates. Inset: optical image of the graphene electrode. Scale bar: 10 μm. (b) Plot of E *vs* log[($i_{ss} - i$)/i] (black dots). Red line is a linear fit to the data. (c) Fit of Butler−Volmer kinetics (eq 2) to the experimental voltammogram (scan rate = 0.02 V/s) for different k^0 values. Inset: close-up view of the dashed square region in the main figure.

effective area of this graphene electrode to be 117 ± 8 μm^2. This result corresponds well to the geometric area we measured from the AFM image (130 μm^2) and provides evidence that the redox reaction occurs on the clean graphene surface. Significant contamination, especially by irreversibly adsorbed species, on the graphene surface would lower the A_{eff},[14] although this measurement may not be sensitive to non-uniform small contaminants scattered across the surface.[36] Any current leakage outside the lithographically defined graphene window would increase the calculated A_{eff}.

The ultramicroelectrode geometry allows fast reaction kinetics to be measured using voltammetry.[10,11] A plot of E *versus* log[($i_{ss} - i$)/i], where i corresponds to the current measured at an applied potential E, is commonly used to characterize the reversibility of the kinetics for ultramicroelectrodes. For a reversible one-electron transfer reaction in which the reaction

rate is much greater than the rate of mass transport, this plot should be linear with a slope of ≈59 mV.[11] As the reaction rate is reduced relative to the mass transport rate, the slope increases. Figure 3b presents a plot of *E versus* log[(i_{ss} − i)/i] measured at an exfoliated graphene device. As is evident from the figure, linearity was very good, and the slope was 58.3 ± 0.3 mV, from which we conclude that the heterogeneous reaction rate of FcMeOH at the graphene surface is much greater than the mass transport rate. We can estimate a *lower limit* for the standard heterogeneous charge transfer rate constant k^0 by fitting the experimental voltammograms to the Bulter−Volmer model, in which the oxidative current for a one-step, one electron process is[11]

$$i_{BV} = \frac{i_{ss}}{1 + e^{-F(E-E_0')/RT} + \left(\frac{FA_{eff}C_0^*}{i_{ss}}k^0\right)^{-1} e^{-F(1-\alpha)(E-E_0')/RT}} \quad (2)$$

where R is the molar gas constant, T is the absolute temperature, E is the applied potential, E_0' is the formal potential of the redox couple, and α is the transfer coefficient. Figure 3c shows the best fits of eq 2 to the experimental data with different fixed k^0 values. E_0' and α are used as fitting parameters, with α being confined to be between 0.3 and 0.7[11,14] and i_{ss} fixed to be 9.01 nA. The fitting quality increases monotonically as the k^0 value increases. Satisfactory fits are obtained for k^0 values larger than ∼0.5 cm/s. We thus estimate the lower limit of k^0 for FcMeOH at the mechanically exfoliated graphene electrode to be ∼0.5 cm/s. Simple estimations based on the observation that the ultramicroelectrode voltammogram is reversible[10,37] also gave similar lower bounds of k^0 of 0.2−0.6 cm/s.

We also investigated the electrochemical properties of CVD-grown graphene electrodes. Figure 4a shows the cyclic voltammograms measured at a CVD graphene electrode in FcMeOH solution at different scan rates. Peak-shaped voltammograms are observed, as expected, given the larger area (0.19 mm^2) of the CVD graphene electrode relative to the exfoliated graphene ultramicroelectrode discussed above. Due to the significant currents (∼1 μA) in this measurement, for a detailed analysis, one should correct for the effect of uncompensated and/or other sources of resistance.[11] Given the three-electrode measurement configuration and supporting electrolyte concentration (0.1 M KCl) in the solution, the resistance from the solution is negligible. Thus the major source of resistance comes from the contact resistance between the metal leads and the graphene sheet, which is ∼1100 Ohm for the device presented in Figure 4. We performed the resistance correction as described in ref 11, and the resulting peak currents (i_p) are plotted in the inset of Figure 4a as a function of the square root of the scan rate ($v^{1/2}$) in which good linearity was observed. Using

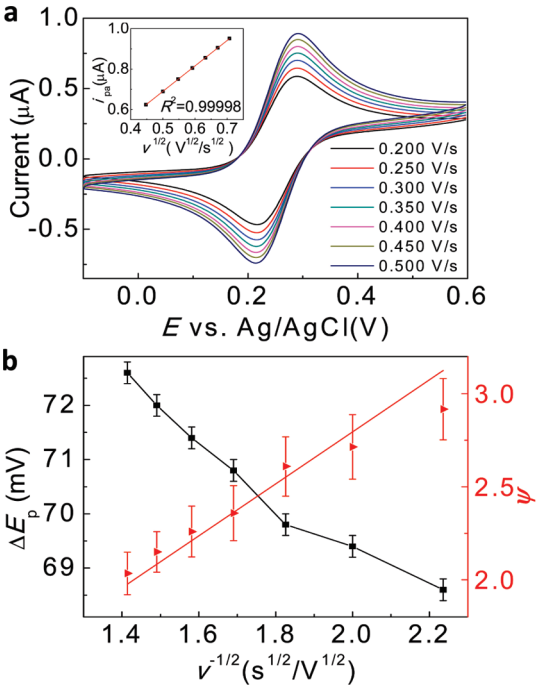

Figure 4. Electrochemistry at a CVD graphene electrode. (a) Cyclic voltammograms of FcMeOH (1 mM) in H_2O/0.1 M KCl measured at a CVD graphene electrode at different potential scan rates. Inset: plot of the anodic peak current (i_p) *versus* the square root of the potential scan rate ($v^{1/2}$). (b) Peak separation ΔE_p and Nicholson's kinetic parameter ψ *versus* the reciprocal of the square root of the potential scan rate ($v^{-1/2}$). A linear fit is used to determine the standard heterogeneous charge transfer rate constant (k^0).

the Randles-Sevcik equation,[11] the effective surface area of the graphene electrode was estimated to be 0.172 ± 0.006 mm^2. This, again, is in reasonable accord with the geometric area of this electrode (0.19 mm^2), indicating that the redox reactions occur predominantly on a clean graphene surface.

Kinetic parameters for the reaction of FcMeOH with CVD graphene can be measured from the potential difference between the oxidation and reduction peaks (ΔE_p) as a function of the scan rate.[9,11] As shown in Figure 4b, ΔE_p (after proper resistance correction) ranges from 68.6 to 72.6 mV and increases at higher scan rate, indicative of quasi-reversible kinetics in the system. Following Nicholson's working curve,[9,11] these ΔE_p values can be converted into a dimensionless kinetic parameter ψ that is directly proportional to the reciprocal of the square root of scan rate, $v^{-1/2}$:

$$\psi = k^0\sqrt{RT/(\pi nFD)}v^{-1/2} \quad (3)$$

The standard heterogeneous rate constant k^0 can thus be determined from a linear fit to the $\psi - v^{-1/2}$ relationship (Figure 4b). From the slope, we find k^0 to be 0.042 ± 0.002 cm/s. To make sure that the relatively high k^0 value we obtained on the CVD graphene electrode is not an artifact resulting from overcorrection of resistance, we have also calculated k^0 without resistance correction. A k^0 value of 0.037 cm/s was determined,

which is ~90% of the k^0 (0.042 cm/s) obtained with resistance correction, indicating that the resistance correction only has a minor effect on the final k^0 value.

Our values of k^0 measured on graphene surfaces can be compared to values from other types of sp^2 carbon surfaces. Using similar experimental and analysis methods, we found the k^0 value of FcMeOH at the basal plane of a freshly prepared bulk graphite electrode to be 0.007 cm/s; k^0 for a similar ferrocene derivative, ferrocenedicarboxylic acid [$Fc(COOH)_2$], at the basal plane of graphite has been reported to be 0.003 cm/s.[38,39] These values are about 1 order of magnitude smaller than the k^0 we measured at the CVD graphene electrode (0.042 cm/s) and 2 orders of magnitude smaller than the k^0 we measured on mechanically exfoliated graphene (>~0.5 cm/s). However, even larger values of k^0 have been measured for ferrocene derivatives at single-wall carbon nanotubes (SWCNTs), which can be regarded as wrapped graphene sheets: for FcMeOH on SWCNTs, $k^0 = 1.1 \pm 0.4$ cm/s,[40] and for ferrocenylmethyltrimethylammonium ($FcTMA^+$) on SWCNTs, $k^0 = 4 \pm 2$ cm/s.[14] Recent studies on graphene pastes have also suggested that graphene may have favorable electron transfer kinetics when compared to graphite.[17−21] The enhanced k^0 is likely related to the observations that graphene (and SWCNTs) has dramatically enhanced chemical reactivity when compared to the basal plane of bulk graphite.[5,6,41] This enhancement is generally believed to be a consequence of the large intrinsic corrugations[30,31] of graphene sheets that are not present in the atomically flat surfaces of bulk graphite. The corrugations lead to considerable curvature and strain in graphene sheets at the atomic scale, which, in turn, activate the graphene surface toward chemical reactions.[5,6] Recent theoretical and experimental studies have further indicated that the corrugations in graphene sheets may also create local midgap states,[32,42] which might contribute to the enhancement of k^0.[39] When compared to exfoliated graphene, the relatively smaller k^0 of CVD graphene may be related to its lower electron mobility.[23]

Finally, we have also studied and characterized the adsorption of FcMeOH onto graphene surfaces. After voltammetric measurements using CVD graphene in 1 mM FcMeOH for ~15 min, we rinsed the graphene electrode thoroughly with deionized water and placed it in 0.1 M KCl solution with no added FcMeOH. Figure 5a shows the cyclic voltammograms subsequently measured. We observed oxidation and reduction peaks at potentials similar to those seen in the diffusive voltammograms recorded in FcMeOH solution (Figure 4a). However, the current levels were more than 2 orders of magnitude lower. These peaks were not present in the voltammograms of control CVD graphene electrodes that had not been previously exposed to FcMeOH in pure electrolyte solution without added FcMeOH

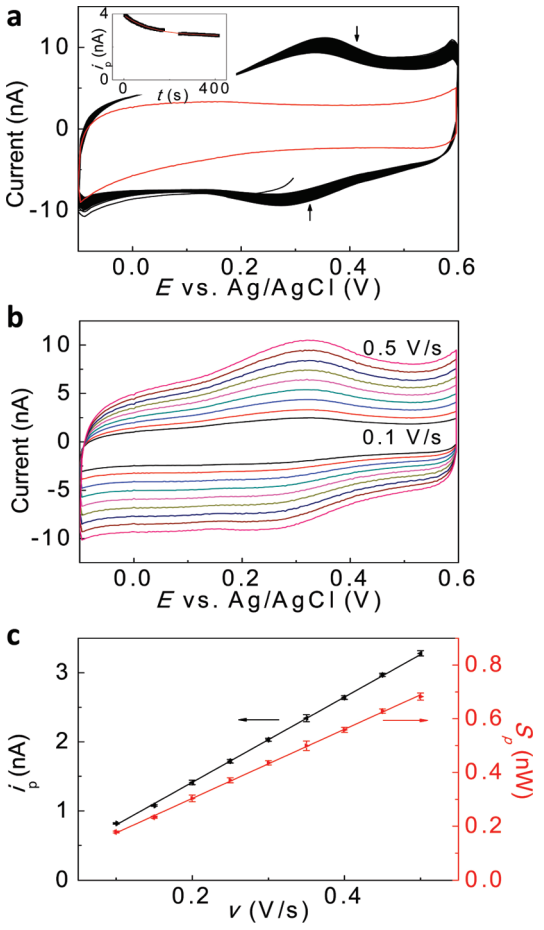

Figure 5. Real-time electrochemical detection of the desorption of FcMeOH from graphene surfaces. (a) Black line: cyclic voltammograms measured on a CVD graphene electrode in 0.1 M KCl solution, after the adsorption of FcMeOH on the graphene surface. Gradual desorption of FcMeOH is observed. Scan rate is 0.4 V/s. Red line: background voltammogram of a control electrode made from the same graphene sheet without FcMeOH adsorption. Inset: decrease of the anodic current peak (i_p) as a function of time. (b) Cyclic voltammograms measured at different scan rates after the desorption process reached equilibrium. Curves from black to pink represent cyclic voltammograms measured at 0.1, 0.15, 0.2, 0.25, 0.3, 0.35, 0.4, 0.45, and 0.5 V/s, respectively. (c) Plot of the anodic peak current (i_p) and peak area (S_p) *versus* the scan rate (v).

(Figure 5a). We conclude that the signals arise from FcMeOH molecules adsorbed onto the CVD graphene surface. In addition, the amplitudes of these peaks decreased during continuous cyclic voltammetric scans on a time scale of ~100 s and tended to stabilize to finite values after ~5 min (Figure 5a inset), indicating that a fraction of the adsorbed FcMeOH molecules can gradually desorb from the surface (likely due to weak adsorption) but that some electrochemically active, irreversibly adsorbed material remains. Figure 5b shows cyclic voltammograms measured at different scan rates after the desorption process had reached a steady state. The peak separations (ΔE_p) at different scan rates ranged from 40 to 54 mV, significantly smaller than the ΔE_p value of *diffusive* cyclic voltammograms

(59 mV),[11] providing additional evidence that the current peaks come from FcMeOH molecules adsorbed onto the graphene surface. Figure 5c presents the anodic peak current (i_p) *versus* scan rate (v) after appropriate background subtractions. The i_p-v curves are linear, as expected[11] for the redox reaction of an adsorbed species. The surface concentration of adsorbed FcMeOH can be estimated based on the area underneath the cyclic voltammetry peaks according to

$$S_p = \int_p i dV = nvFA_{eff}\Gamma \quad (4)$$

where S_p is the area under the peak, A_{eff} is the effective area of the electrode, and Γ is the surface coverage. From a linear fit of the peak areas to the scan rate (Figure 5c), we find $\Gamma = 1.1 \times 10^{-11}$ mol/cm^2. When a ~4.5 Å diameter for FcMeOH molecules is assumed,[43] this corresponds to ~1% of a monolayer coverage on the graphene surface. This value is comparable to what we observe on bulk graphite surfaces (~2% monolayer coverage) but considerably lower than the reported adsorption of ferrocene on glassy carbon electrodes modified by multiwalled carbon nanotubes.[44] We did not detect adsorption of FcMeOH on exfoliated graphene electrodes. Because of the much smaller area of these electrodes, we estimate that this measurement is not sufficiently sensitive when the surface coverage is below ~10%. On the other hand, graphene sheets of larger areas are hard to produce through the standard exfoliation method.[45] The small FcMeOH coverage on CVD graphene suggests that the irreversible adsorption of FcMeOH occurs primarily at local defect sites.

CONCLUSIONS

In conclusion, we have performed electrochemical studies of individual monolayer graphene sheets derived from both mechanically exfoliated graphene and CVD graphene. Careful device design ensured that all redox reactions occur on clean graphene surfaces within well-defined areas. We found that the electron transfer rates of graphene electrodes are more than 10-fold faster than the basal plane of bulk graphite, likely due to the presence of corrugations in the graphene sheets. We also demonstrated the electrochemical detection of (likely irreversible) adsorption of FcMeOH onto CVD graphene. Our results demonstrate that electrochemistry provides a powerful means to investigate the interactions between molecules and the surfaces of graphene sheets used as electrodes.

EXPERIMENTAL METHODS

Fabrication of Graphene Electrodes. Mechanically exfoliated graphene sheets were extracted from Kish graphite flakes and deposited onto Si wafers with a 300 nm thermal oxide through the standard "scotch tape" method.[45] CVD graphene sheets were grown on 25 μm thick copper foils using methane and hydrogen[23] and transferred onto the SiO_2-Si substrate following the procedure described in ref 24. The graphene sheet was connected by two metal leads (1 nm Cr/50 nm Au) at one end using optical lithography (Figure 1a). To isolate the metal leads from the electrolyte solution, a 100 nm Al_2O_3 layer was deposited by e-beam evaporation at a deposition rate of ~1 Å/s (Figure 1b), followed by a 600 nm thick layer of parylene (Figure 1c). To expose the graphene surface, an oxygen plasma was employed to pattern the parylene layer (Figure 1d), and a window was opened in the Al_2O_3 layer through a wet etch using AZ 300 MIF photoresist developer (Figure 1e). In the final step, vacuum annealing at 350 °C was used to remove possible residuals on the graphene surface.

Raman and AFM Characterization. The Raman spectra were recorded with a Renishaw InVia micro-Raman system using a 488 nm laser and a 2400 lines/mm grating. A confocal microscope with a 50× objective lens was used to record spectra at a spatial resolution of ~2 μm. AFM characterization was performed on a Veeco Dimension 3100 AFM in tapping mode with an Olympus tip. Typical values for the force constant, resonance frequency, and tip radius were 42 N/m, 340 kHz, and <10 nm, respectively.

Electrochemical Measurements. Cyclic voltammograms were measured in a three-electrode configuration using a CH Instrument model 900 potentiostat. The fabricated graphene electrode was used as the working electrode. Ag/AgCl (saturated KCl) and Pt were used as the reference and counter electrodes, respectively. A micromanipulator was used to smoothly insert the graphene electrode into the solution. The cell was placed in a Faraday cage on top of an optical table to reduce electronic and acoustic noise.

Acknowledgment. The authors thank Prof. Paul McEuen, Samantha Roberts, and Arend van der Zande for help in CVD graphene device design, and Dr. Ke Xu, Dr. Joshua Parks, Sufei Shi, and Eugenia Tam for helpful discussions. The research was supported by the Cornell Center for Chemical Interfacing, a Phase I Center for Chemical Innovation (NSF/CHE-0847926). We also acknowledge NSF support through use of the Cornell Nanofabrication Facility/NNIN and the Cornell Center for Materials Research facilities.

REFERENCES AND NOTES

1. Geim, A. K.; Novoselov, K. S. The Rise of Graphene. *Nat. Mater.* **2007,** *6*, 183–191.
2. Geim, A. K. Graphene: Status and Prospects. *Science* **2009,** *324*, 1530–1534.
3. Schedin, F.; Geim, A. K.; Morozov, S. V.; Hill, E. W.; Blake, P.; Katsnelson, M. I.; Novoselov, K. S. Detection of Individual Gas Molecules Adsorbed on Graphene. *Nat. Mater.* **2007,** *6*, 652–655.
4. Wehling, T. O.; Novoselov, K. S.; Morozov, S. V.; Vdovin, E. E.; Katsnelson, M. I.; Geim, A. K.; Lichtenstein, A. I. Molecular Doping of Graphene. *Nano Lett.* **2008,** *8*, 173–177.
5. Ryu, S.; Han, M. Y.; Maultzsch, J.; Heinz, T. F.; Kim, P.; Steigerwald, M. L.; Brus, L. E. Reversible Basal Plane Hydrogenation of Graphene. *Nano Lett.* **2008,** *8*, 4597–4602.
6. Elias, D. C.; Nair, R. R.; Mohiuddin, T. M. G.; Morozov, S. V.; Blake, P.; Halsall, M. P.; Ferrari, A. C.; Boukhvalov, D. W.; Katsnelson, M. I.; Geim, A. K.; Novoselov, K. S. Control of Graphene's Properties by Reversible Hydrogenation: Evidence for Graphane. *Science* **2009,** *323*, 610–613.
7. Sharma, R.; Baik, J. H.; Perera, C. J.; Strano, M. S. Anomalously Large Reactivity of Single Graphene Layers and Edges toward Electron Transfer Chemistries. *Nano Lett.* **2010,** *10*, 398–405.

8. Wang, Q. H.; Hersam, M. C. Room-Temperature Molecular-Resolution Characterization of Self-Assembled Organic Monolayers on Epitaxial Graphene. *Nat. Chem.* **2009,** *1*, 206–211.
9. Nicholson, R. S. Theory and Application of Cyclic Voltammetry for Measurement of Electrode Reaction Kinetics. *Anal. Chem.* **1965,** *37*, 1351–1355.
10. Oldham, K. B.; Myland, J. C.; Zoski, C. G.; Bond, A. M. Kinetic-Parameters from Steady-State Voltammograms at Microdisc Electrodes. *J. Electroanal. Chem.* **1989,** *270*, 79–101.
11. Bard, A. J.; Faulkner, L. R. *Electrochemical Methods: Fundamentals and Applications*, 2nd ed.; Wiley: New York, 2000.
12. McCreery, R. L. Advanced Carbon Electrode Materials for Molecular Electrochemistry. *Chem. Rev.* **2008,** *108*, 2646–2687.
13. Campbell, J. K.; Sun, L.; Crooks, R. M. Electrochemistry Using Single Carbon Nanotubes. *J. Am. Chem. Soc.* **1999,** *121*, 3779–3780.
14. Heller, I.; Kong, J.; Heering, H. A.; Williams, K. A.; Lemay, S. G.; Dekker, C. Individual Single-Walled Carbon Nanotubes as Nanoelectrodes for Electrochemistry. *Nano Lett.* **2005,** *5*, 137–142.
15. Chlistunoff, J.; Cliffel, D.; Bard, A. J. Electrochemistry of Fullerene Films. *Thin Solid Films* **1995,** *257*, 166–184.
16. Pleskov, Y. V. Electrochemistry of Diamond: A Review. *Russ. J. Electrochem.* **2002,** *38*, 1275–1291.
17. Shao, Y. Y.; Wang, J.; Wu, H.; Liu, J.; Aksay, I. A.; Lin, Y. H. Graphene Based Electrochemical Sensors and Biosensors: A Review. *Electroanalysis* **2010,** *22*, 1027–1036.
18. Tang, L. H.; Wang, Y.; Li, Y. M.; Feng, H. B.; Lu, J.; Li, J. H. Preparation, Structure, and Electrochemical Properties of Reduced Graphene Sheet Films. *Adv. Funct. Mater.* **2009,** *19*, 2782–2789.
19. Alwarappan, S.; Erdem, A.; Liu, C.; Li, C. Z. Probing the Electrochemical Properties of Graphene Nanosheets for Biosensing Applications. *J. Phys. Chem. C* **2009,** *113*, 8853–8857.
20. Zhou, M.; Zhai, Y. M.; Dong, S. J. Electrochemical Sensing and Biosensing Platform Based on Chemically Reduced Graphene Oxide. *Anal. Chem.* **2009,** *81*, 5603–5613.
21. Wang, Y.; Shao, Y. Y.; Matson, D. W.; Li, J. H.; Lin, Y. H. Nitrogen-Doped Graphene and Its Application in Electrochemical Biosensing. *ACS Nano* **2010,** *4*, 1790–1798.
22. Murray, R. Roses and Raspberries. *Anal. Chem.* **2010,** *82*, 3405–3405.
23. Li, X. S.; Cai, W. W.; An, J. H.; Kim, S.; Nah, J.; Yang, D. X.; Piner, R.; Velamakanni, A.; Jung, I.; Tutuc, E.; Banerjee, S. K.; Colombo, L.; Ruoff, R. S. Large-Area Synthesis of High-Quality and Uniform Graphene Films on Copper Foils. *Science* **2009,** *324*, 1312–1314.
24. Li, X. S.; Zhu, Y. W.; Cai, W. W.; Borysiak, M.; Han, B. Y.; Chen, D.; Piner, R. D.; Colombo, L.; Ruoff, R. S. Transfer of Large-Area Graphene Films for High-Performance Transparent Conductive Electrodes. *Nano Lett.* **2009,** *9*, 4359–4363.
25. Xia, J. L.; Chen, F.; Li, J. H.; Tao, N. J. Measurement of the Quantum Capacitance of Graphene. *Nat. Nanotechnol.* **2009,** *4*, 505–509.
26. Ferrari, A. C.; Meyer, J. C.; Scardaci, V.; Casiraghi, C.; Lazzeri, M.; Mauri, F.; Piscanec, S.; Jiang, D.; Novoselov, K. S.; Roth, S.; Geim, A. K. Raman Spectrum of Graphene and Graphene Layers. *Phys. Rev. Lett.* **2006,** *97*, 187401.
27. Levendorf, M. P.; Ruiz-Vargas, C. S.; Garg, S.; Park, J. Transfer-Free Batch Fabrication of Single Layer Graphene Transistors. *Nano Lett.* **2009,** *9*, 4479–4483.
28. Lee, Y.; Bae, S.; Jang, H.; Jang, S.; Zhu, S. E.; Sim, S. H.; Song, Y. I.; Hong, B. H.; Ahn, J. H. Wafer-Scale Synthesis and Transfer of Graphene Films. *Nano Lett.* **2010,** *10*, 490–493.
29. Cao, H. L.; Yu, Q. K.; Jauregui, L. A.; Tian, J.; Wu, W.; Liu, Z.; Jalilian, R.; Benjamin, D. K.; Jiang, Z.; Bao, J.; Pei, S. S.; Chen, Y. P. Electronic Transport in Chemical Vapor Deposited Graphene Synthesized on Cu: Quantum Hall Effect and Weak Localization. *Appl. Phys. Lett.* **2010,** *96*, 122106.
30. Meyer, J. C.; Geim, A. K.; Katsnelson, M. I.; Novoselov, K. S.; Booth, T. J.; Roth, S. The Structure of Suspended Graphene Sheets. *Nature* **2007,** *446*, 60–63.
31. Ishigami, M.; Chen, J. H.; Cullen, W. G.; Fuhrer, M. S.; Williams, E. D. Atomic Structure of Graphene on SiO_2. *Nano Lett.* **2007,** *7*, 1643–1648.
32. Xu, K.; Cao, P. G.; Heath, J. R. Scanning Tunneling Microscopy Characterization of the Electrical Properties of Wrinkles in Exfoliated Graphene Monolayers. *Nano Lett.* **2009,** *9*, 4446–4451.
33. Novoselov, K. S.; Geim, A. K.; Morozov, S. V.; Jiang, D.; Zhang, Y.; Dubonos, S. V.; Grigorieva, I. V.; Firsov, A. A. Electric Field Effect in Atomically Thin Carbon Films. *Science* **2004,** *306*, 666–669.
34. Heinze, J. Ultramicroelectrodes in Electrochemistry. *Angew. Chem., Int. Ed. Engl.* **1993,** *32*, 1268–1288.
35. Guo, J. D.; Amemiya, S. Permeability of the Nuclear Envelope at Isolated Xenopus Oocyte Nuclei Studied by Scanning Electrochemical Microscopy. *Anal. Chem.* **2005,** *77*, 2147–2156.
36. Dumitrescu, I.; Unwin, P. R.; Wilson, N. R.; Macpherson, J. V. Single-Walled Carbon Nanotube Network Ultramicroelectrodes. *Anal. Chem.* **2008,** *80*, 3598–3605.
37. Mirkin, M. V.; Bard, A. J. Simple Analysis of Quasi-Reversible Steady-State Voltammograms. *Anal. Chem.* **1992,** *64*, 2293–2302.
38. Nielson, R. M.; McManis, G. E.; Safford, L. K.; Weaver, M. J. Solvent and Electrolyte Effects on the Kinetics of Ferrocenium Ferrocene Self-Exchange—A Reevaluation. *J. Phys. Chem.* **1989,** *93*, 2152–2157.
39. Cline, K. K.; McDermott, M. T.; McCreery, R. L. Anomalously Slow-Electron Transfer at Ordered Graphite-Electrodes—Influence of Electronic Factors and Reactive Sites. *J. Phys. Chem.* **1994,** *98*, 5314–5319.
40. Patil, A. V.; Beker, A. F.; Wiertz, F. G. M.; Heering, H. A.; Coslovich, G.; Vlijm, R.; Oosterkamp, T. H. Fabrication and Characterization of Polymer Insulated Carbon Nanotube Modified Electrochemical Nanoprobes. *Nanoscale* **2010,** *2*, 734–738.
41. Niyogi, S.; Hamon, M. A.; Hu, H.; Zhao, B.; Bhowmik, P.; Sen, R.; Itkis, M. E.; Haddon, R. C. Chemistry of Single-Walled Carbon Nanotubes. *Acc. Chem. Res.* **2002,** *35*, 1105–1113.
42. Guinea, F.; Katsnelson, M. I.; Vozmediano, M. A. H. Midgap States and Charge Inhomogeneities in Corrugated Graphene. *Phys. Rev. B* **2008,** *77*, 075422.
43. Williams, M. E.; Hupp, J. T. Scanning Electrochemical Microscopy Assessment of Rates of Molecular Transport through Mesoporous Thin-Films of Porphyrinic "Molecular Squares". *J. Phys. Chem. B* **2001,** *105*, 8944–8950.
44. Zheng, D.; Li, H. H.; Lu, B. Y.; Xu, Z. H.; Chen, H. Y. Electrochemical Properties of Ferrocene Adsorbed on Multi-walled Carbon Nanotubes Electrode. *Thin Solid Films* **2008,** *516*, 2151–2157.
45. Novoselov, K. S.; Jiang, D.; Schedin, F.; Booth, T. J.; Khotkevich, V. V.; Morozov, S. V.; Geim, A. K. Two-Dimensional Atomic Crystals. *Proc. Natl. Acad. Sci. U.S.A.* **2005,** *102*, 10451–10453.